NASA Technical Memorandum 86934

Characterization of Erosion of Metallic Materials Under Cavitation Attack in a Mineral Oil

Bezzam C.S. Rao and Donald H. Buckley
Lewis Research Center
Cleveland, Ohio

Prepared for the
Tribology Conference
cosponsored by the American Society of Lubrication Engineers
and the American Society of Mechanical Engineers
Atlanta, Georgia, October 8-10, 1985

NASA

CHARACTERIZATION OF EROSION OF METALLIC MATERIALS UNDER CAVITATION ATTACK IN A MINERAL OIL

Bezzam C. S. Rao* and Donald H. Buckley†
National Aeronautics and Space Administration
Lewis Research Center
Cleveland, Ohio

Abstract

Cavitation erosion and erosion rates of eight metallic materials representing three crystal structures were studied. The erosion experiments were conducted with a 20-kHz ultrasonic magnetostrictive oscillator in a viscous mineral oil. The erosion rates of the metals with an fcc matrix were 10 to 100 times higher than that of an hcp-matrix titanium alloy. The erosion rates of iron and molybdenum, with bcc matrices, were higher than that of the titanium alloy but lower than those of the fcc materials. Studies with scanning electron microscopy indicated that the cavitation pits were initially formed at the grain boundaries and precipitates and that the pits formed at the junction of grain boundaries grew faster than the others. Transcrystalline craters formed by cavitation attack over the surface of grains and roughened the surfaces by multiple slip and twinning. Surface roughness measurements showed that the pits that formed over the grain boundaries deepened faster than other pits. Computer analysis revealed that a geometric expression describes the nondimensional erosion curves during the time period $0.5\ t_0 < t < 2.5\ t_0$, where t_0 is the incubation period. The fcc metals had very short incubation periods; the titanium alloy had the longest incubation period.

---

*Case Western Reserve University, Cleveland, Ohio and NASA Resident Research Associate.

†Member, ASLE.

INTRODUCTION

Cavitation - the formation, growth, and collapse of vapor bubbles - is known to occur in all liquids and liquid metals in many engineering situations. The occurrence of cavitation in a system has many undesirable effects. The erosion of boundary material is one of these effects that has been faced by the engineering profession over the past 4 or 5 decades. Pumps, turbines, gates, valves, ship propellers, bearings, seals, gears, and many other engineering devices are known to suffer from this phenomenon. The situation may involve a thin layer of liquid, as in lubrication between two surfaces, or a large quantity of flowing liquid, as in flow past a valve or through a turbine. The mechanisms of cavitation attack and material removal are the same in all such situations. Many investigations (1) over the past 3 or 4 decades have covered several aspects of the phenomenon that can be broadly classified as the inception, growth, and collapse of vapor bubbles, the pressures generated and the damage caused to the adjoining boundary materials.

In spite of these investigations, a precise understanding of these subjects has still not been achieved. The highly transient nature of the events and the submicroscopic details of the attack are largely responsible for the difficulties in achieving a complete understanding. In addition, materials differ in their response to cavitation attack . The information available concerning erosion in viscous liquids of engineering importance is very limited. The few attempts to generalize the response of different materials to cavitation attack (2-6) had only partial success when a large spectrum of materials was considered and indicated the need for a better understanding of the phenomenon.

This paper presents investigations concerning the erosion and erosion rate of different metallic materials in a viscous mineral oil. The materials

studied had three crystal structures. The formation and growth of cavitation pits were studied by scanning electron microscopy and surface roughness measurements. Attempts to describe the first two regions of the erosion curves with a generalized mathematical expression are presented.

EXPERIMENTAL EQUIPMENT AND TEST MATERIALS

The experiments were carried out in an ultrasonic electrostrictive oscillator (Fig. 1) operating at 20-kHz frequency and with a peak-to-peak amplitude of 50 μm. The test specimen was mounted at the tip of the horn and immersed in the mineral oil. The test specimen vibrated with the horn as it expanded and contracted with the electrostrictive action of the converter. This action created a low-pressure region and hence caused cavitation of the liquid over the surface of the test specimen. The test specimens for the experiments were prepared from 12.7-mm-diameter rods. Five metals with face-centered-cubic (fcc) matrices, viz aluminum 6061-T6, copper (electrolytic tough pitch), free cutting brass, phosphor bronze, and nickel; two metals with body-centered-cubic (bcc) matrices, viz iron and molybdenum; and titanium (Ti-5Al-2.5Sn), with a hexagonal-close-packed (hcp) matrix, were examined in the study. The chemical composition and density of these materials are presented in Table 1. The experiments were carried out in a mineral oil whose physical properties are given in Table 2. To examine the role of liquid viscosity in cavitation, a thick (high viscosity) mineral oil was selected for the investigation.

The surfaces of the specimens were initially polished with fine emery papers and then with 0.5- and 0.05-μm alumina powders in a polishing machine. The materials were examined in the as-received condition and were not heat treated.

THEORETICAL CONSIDERATIONS

The erosion of metallic materials by cavitation involves the impact on the surface of microjets or shock waves formed during the collapse of the cavitation bubbles. In a recent study, Shima et al. (7) observed that, depending on the distance of the solid boundary from the center of bubble collapse, either a shock wave, a microjet, or a combination of the two was responsible for the impact pressure exerted on the solid wall. Many investigators (8) have shown that during the nonspherical collapse of the cavitation bubbles, thin, high-velocity microjets are generated.

The growth and collapse of the cavitation bubbles are influenced by the viscosity of the liquid. The role of viscosity in the dynamics of cavitation bubbles and in the pressures generated in the liquid is discussed in detail in Ref. (9).

The materials respond to this attack according to their microstructure, strength, and material properties. Since the microjets striking the surface are submicroscopic, it is reasonable to expect that the microstructure of the material is very important in its response to such an attack. The typical structure of a polycrystalline material based on the example of iron is reproduced in Fig. 2. Several metallographic features and the general surface defects are shown. A network of microjets repeatedly attacks the surface at a given frequency. In most situations, the microjets are smaller than the grains, and hence each grain is attacked by one or two microjets. Some of the microjets strike over the grain boundaries. The attack on grains results in plastic deformation involving slip, twinning, shear bands, etc. Some amount of erosion during early attack may also be expected from grain boundary precipitates, point defects, and other surface imperfections.

The applied stress σ and the critical resolved shear stress τ_0 are related to the shear stress τ_d required to operate a slip source according to the equation

$$\tau_d = \frac{1}{M}\left(\frac{\sigma}{M} - \tau_0\right)\left(\frac{d}{x}\right)^{1/2} \qquad (1)$$

where

M orientation factor, $1/\sin\phi\cos\lambda$

d average grain diameter

x distance between point of stress and point where slip is to be initiated

ϕ angle between slip plane and stress axis

λ angle between slip direction and stress axis

In a given cavitation situation, the applied stress σ is a constant. The orientation factor M varies with the crystal structure of the material; its average values according to Sach's model are 2.24, 2.0, and 6.5 for fcc, bcc, and hcp polycrystals, respectively. According to Taylor's model M is 3.06 for fcc polycrystals (11). The observation of deformation twins under cavitation attack (12,13) suggests that stacking faults are generated in the material during cavitation attack. Materials with high stacking fault energy γ would be expected to erode faster under cavitation attack.

The considerations discussed in the preceding paragraphs indicate that the orientation factor M, the critical resolved shear stress τ_0, and the stacking fault energy γ are very important parameters governing the deformation of metals and alloys under cavitation attack.

EROSION OF THE MATERIALS

Mean Depth of Penetration

The erosion of materials is expressed as the mean depth of penetration (MDP) from the surface. The MDP is computed from the mass loss measurements of the test specimens according to the equation

$$MDP = \frac{\text{Mass loss per unit area}}{\text{Density}} \qquad (2)$$

The variation of the mean depth of penetration of the eight metals for a total test time of 40 min is presented in Fig. 3. The erosion on molybdenum and Ti-5Al-2.5Sn was insignificant. The MDP variation of these two materials to a test time of 1800 min is presented in Fig. 4. The MDP of iron is also shown in Fig. 4 to compare the time scale of erosion with that of the materials presented in Fig. 3. Copper had the largest MDP (Fig. 3) and Ti-5Al-2.5Sn had the smallest MDP (Fig. 4). The other metals Al 6061-T6, brass, nickel, iron, phosphor bronze, and molybdenum have intermediate MDP's in decreasing order of magnitude.

The variation and average values of the mean depth of penetration rate (MDPR) with time were plotted for the eight metals. The average MDPR of the fcc group (Fig. 5(a)) varied from 26.4 μm/hr for phosphor bronze to 542.3 μm/hr for copper. The average MDPR's for iron and molybdenum (Fig. 5(b)) were 43 and 1.95 μm/hr, respectively; tnat for Ti-5Al-2.5Sn (Fig. 5 (c)) was 0.5 μm/hr. The MDPR's of the fcc group were 10 to 100 times higher than the erosion rate of the hcp-matrix material Ti-5Al-2.5Sn. Similarly, the MDPR's of iron and molybdenum (bcc matrices) were higher than the erosion rate of Ti-5Al-2.5Sn. The MDPR's of both fcc and hcp materials in general peaked and then decreased. Ti-5Al-2.5Sn had periods of low or insignificant MDPR followed by periods of high MDPR (Fig. 5(c)). For the bcc materials (Fig. 5(b)) the MDPR increased steadily as the test duration increased. The experiments on these materials could not be carried out for a longer duration because the specimens broke from the horn.

Scanning Electron Microscopy Observations

To clarify the processes of deformation and material removal under cavitation attack, the eroded surfaces were examined with a scanning electron

microscope. Micrographs presented in Fig. 6 show the different stages of these processes for Cu-35.5Zn-3Pb brass. On the undamaged, lightly etched surface (Fig. 6(a)) the lead phase is evident from the dark spots over the grain boundaries. The eroded surface at 10 s (Fig. 6(b)) shows the formation of tiny cavitation pits over the grain boundaries and precipitates. The eroded surface at 20 s (Fig. 6(c)) shows further cavitation attack over the grain boundaries and plastic deformation of the grains involving slip. The eroded surface at 30 s (Fig. 6(d)) shows growth in the size of cavitation pits at the junction of grain boundaries and the formation of deformation twins. The eroded surface at 40 s (Fig. 6(e)) shows material removal by fragmentation of the grain. The fragmented particle is bounded by the grain boundaries and possibly a twin plane. An indentation due to the possible impact of a microjet can also be seen above the fragmented particle. The eroded surface at 60 s (Fig. 6(f)) shows a considerable amount of deformation and the formation of large craters on the surface grains.

Figure 7 presents magnified views of individual cavitation pits at different stages of cavitation attack. Figures 7(a) to (d) are magnified views of Figs. 6(c) to (f), respectively. Figures 7(a) and (b) show cavitation pit growth caused by cutting action along the grain boundaries and through specific planes in the grains. Note that the cutting action into the grain resulted in progressive slip and twinning across the grain. Figure 7(c) shows clearly the details of the fragmented particle and the indentation on its surface. Figure 7(d) presents the development of a transcrystalline crater.

The investigations using scanning electron microscopy, in general, revealed that cavitation pits were initially formed over the grain boundaries and other precipitates. The pits that formed at the junction of three or more grain boundaries appeared to grow faster than the other pits by cutting action

along the grain boundaries and into the grain. Multiple slip and twinning occurred across the grains. Part of the grains close to the triple points eroded by fragmentation. Cavitation attack over the surface of grains roughened by multiple slip and twinning formed transcrystalline craters. The nature of the indentations over the surface and the pits formed suggested the cylindrical impact of a microjet during cavitation attack rather than the spherical impact of a shock wave.

Surface Roughness Measurements

The variations in surface roughness during cavitation attack were studied by taking surface profiles at different intervals. Comparing two typical profiles of the Ti-5Al-2.5Sn surface at 660 and 1440 min (Fig. 8) with the micrographs presented in Figs. 6 and 7 suggested that the deep pits in the surface profiles were located over the grain boundaries. They deepened faster than the craters formed over grain surfaces. The maximum depths h_{max} of the pits in the surface profiles were 6 and 10 μm at 660 and 1440 min, respectively. The MDP obtained from mass loss measurements at these two times were 5.7 and 13.1 μm, respectively. For the titanium alloy, the two quantities h_{max} and MDP were of comparable magnitude. But, for the materials with fcc and bcc matrices, h_{max} was much larger than MDP.

FITTING AN EQUATION FOR THE EROSION DATA

To clarify the variation of erosion (MDP) with increasing cavitation attack, different mathematical expressions were used to describe the experimental data. This was achieved by using a "curve fitter" program developed by Interactive Microware Inc. (14) with an Apple II personal computer. This program can fit an equation by either interpolation or least-squares techniques. A least-squares technique is the most reasonable approach for the type of experimental data in this study. With this program

either linear, geometric, exponential, or polynomial expressions can be fitted. The different forms of these expressions are

$$\text{Linear:} \quad y = Ax \tag{3}$$

$$\text{Geometric:} \quad y = Ax^B \tag{4}$$

$$\text{Exponential:} \quad y = A \exp(Bx) \text{ or } Ae^{Bx} \tag{5}$$

$$\text{Polynomial:} \quad y = A + Bx + Cx^2 + \text{---} Px^n \tag{6}$$

where n is the selected degree of the equation and $n + 1$ is the number of terms.

The erosion curves presented in Figs. 3 to 5 indicate three regions, viz, (1) an initial region of very low or insignificant erosion rate; (2) a region of increasing erosion rate; and (3) a region of decreasing erosion rate. The erosion curves of iron and molybdenum show only the first two regions. The initial region is generally termed the "incubation period." The decreasing erosion rate, in the third region, is perhaps due to the impact pressures of the microjets or shock waves being attenuated in traveling longer distances as erosion progresses. The following analysis is confined to the first two regions of erosion curves.

To generalize the variation of erosion on different materials, it is necessary to use nondimensional experimental data. In the present analysis, the incubation period t_0 and the corresponding mean depth of penetration (MDPO) of the different materials were used to nondimensionalize the time t and the MDP, respectively. The nondimensional quantities can be expressed as

$$\text{MDPN} = \frac{\text{MDP}}{\text{MDPO}} \tag{7}$$

$$T = \frac{t}{t_0} \tag{8}$$

The incubation period t_0 is generally defined in three ways, viz (1) the duration of a test in which no mass loss occurs; (2) the intercept on the time

axis as the linear part of the erosion curve is extended to it; and (3) the duration of a test for obtaining a defined value of MDP (e.g., 2 or 5 μm). The first definition is mostly hypothetical because the erosion of precipitates and other surface defects is known to occur in relatively insignificant periods of cavitation attack. In the present analysis incubation periods defined according to the second and third definitions were used. The analysis using the incubation periods that corresponded to an MDP of 5 μm, according to the third definition, resulted in better statistical quantities than the analysis using incubation periods obtained according to the second definition. The analysis using nondimensional erosion data involving incubation periods corresponding to an MDP of 5 μm is described in the following paragraphs.

The incubation periods t_0 of the eight materials, the equations obtained with these values, and the corresponding statistical quantities CD, CC, and SE are presented in Table 3. Small changes in the values of t_0 were made in the analysis in order to make the coefficients in the equations as close to unity as possible. For the materials examined in this study the fcc metals had very short incubation periods (Fig. 9), molybdenum (bcc matrix) had a longer period, and the titanium alloy (hcp matrix) had the longest period. An examination of the statistical quantities in Table 3 indicates that a geometric equation of the type of Eq. (4) describes the erosion curves extremely well in the first two regions covering $0.5\ t_0 < t < 2.5\ t_0$ of time.

A plot of the nondimensional quantities MDPN and T (Fig. 10) shows that molybdenum (bcc matrix) eroded fastest in relation to its incubation period and that copper and aluminum (fcc matrices) and titanium (hcp matrix) eroded at considerably slower rates. The same conclusion can be reached by examining the exponents in the best correlating equations presented in Table 3. These

investigations show that the materials with fcc matrices in general had short incubation periods. Therefore most of these materials eroded quickly under cavitation attack. The materials with hcp matrices had long incubation periods and eroded most slowly. The materials with bcc matrices had high erosion rates although they had long incubation periods. Hence, materials with hcp matrices need more detailed investigation to characterize their behavior under cavitation attack and to exploit their strength in cavitation situations.

CONCLUSIONS

The erosion of eight metallic materials due to cavitation attack in a mineral oil was studied. Variations in mean depth of penetration, surface roughness, and microstructure were investigated. From these investigations, the following conclusions were drawn:

1. The erosion rates of the fcc-matrix materials were 10 to 100 times higher than the erosion rate of a titanium alloy (hcp matrix). The erosion rates of iron and molybdenum (bcc matrices) were higher than that of the titanium alloy but lower than those of the fcc group.

2. The erosion rates of both fcc and hcp materials in general indicated a peak rate and then a decreasing trend. Also the erosion of the titanium alloy had periods of low or insignificant mean depth of penetration rate (MDPR) followed by periods of high MDPR. The erosion rate of bcc materials increased with time.

3. Investigations using scanning electron microscopy indicated that cavitation pits were initially formed over the grain boundaries and other precipitates. Part of the grains close to the junction of grain boundaries eroded by fragmentation. Transcrystalline craters formed by cavitation attack over the surface grains that had been roughened by multiple slip and twinning.

4. Measurement of the variations in surface roughness during cavitation attack indicated that the pits formed over the grain boundaries deepened faster than the other pits. The maximum depth of the pits was generally greater than the MDP obtained from mass loss measurements.

5. A geometric expression such as $MDPN = AT^B$ fitted the nondimensional experimental data of the eight materials very well in the range $0.5\ t_0 < t < 2.5\ t_0$, where t_0 is the incubation period. The fcc materials had very short incubation periods, the bcc materials had longer incubation periods, and the titanium alloy had the longest incubation period.

REFERENCES

(1) Hammitt, F.G., Cavitation and Multiphase Flow Phenomena, McGraw Hill, (1980), pp. 220-291.

(2) Thiruvengadam, A., "A Unified Theory of Cavitation Damage," J. Basic Eng., 85, pp. 365-376 (1963).

(3) Garcia, R., and Hammitt, F.G., "Cavitation Damage and Correlations with Material and Fluid Properties," J. Basic Eng., 89, pp. 753-763 (1967).

(4) Rao, B.C.S., Rao, N.S.L., and Seetharamiah, K., "Cavitation Erosion Studies with Venturi and Rotating Disk in Water," J. Basic Eng., 92, pp. 563-579 (1970).

(5) Rao, B.C.S., Rao, P.V., and Rao, N.S.L., "Evaluation of Erosion Resistance of Metallic Materials and the Role of Material Properties in Correlations," J. Test. Eval., 7, pp. 133-146 (1979).

(6) Kristensen, J.K., Hansson, I., and Morch, K.A., "A Simple Model for Cavitation Erosion of Metals," J. Phys. D, 11, pp. 899-912 (1978).

(7) Shima, A., Takayama, K., Tomita, Y., and Ohsawa, N., "Mechanism of Impact Pressure Generation from Spark-Generated Bubble Collapse Near a Wall," AIAA J., 21, pp. 55-59 (1983).

(8) Lauterborn, W., and Bolle, H., "Experimental Investigations of Cavitation-Bubble Collapse in the Neighborhood of a Solid Boundary," J. Fluid Mech., 72, pp. 391-399 (1975).

(9) Rao, B.C.S., and Buckley, D.H., "Cavitation Pitting and Erosion of Aluminum 6061-T6 in Mineral Oil and Water," NASA TP-2146, (1983).

(10) Engel, L., and Klingele, H., An Atlas of Metal Damage, Wolfe Publishing Ltd., London, (1981).

(11) Tegart, W.J.M., Elements of Mechanical Metallurgy, Macmillan, (1966), pp. 99-193.

(12) Rao, B.C.S., and Buckley, D.H., "Deformation and Erosion of FCC Metals and Alloys Under Cavitation Attack," Mater. Sci. Eng., 67, pp. 55-67 (1984).

(13) Pedersen, T.F., Pedersen, S., and Hansson, I., "Sub-surface Deformation Studies of Cavitation Eroded FCC Materials," Proceedings of the 6th International Conference on Erosion by Liquid and Solid Impact, ed. by J.E. Field and N.S. Corney, Cavendish Laboratory, Cambridge England, (1983), pp. 4-1 to 4-7.

(14) Warme, P.K., Curve Fitter, Interactive Microware Inc., State College, PA (1980).

TABLE 1. CHEMICAL COMPOSITION, AVERAGE GRAIN DIAMETER, DENSITY, AND CRYSTAL STRUCTURE OF THE METALS

Material	Composition	Measured average grain diameter, μm	Density, g/cm^3	Crystal structure
Al 6061 T6	Al 1.0Mg 0.6Si 0.25Cu 0.25Cr	20	2.70	fcc
Cu (ETP)	99.95Cu 0.040 O	75	8.89	
Brass	Cu 35.5Zn 3Pb	10	8.50	
Phosphor bronze	Cu 2.6Sn 0.6P 3Pb-0.07Zn	35	8.86	
Nickel	99.9 Percent Ni	(a)	8.90	
Iron	99.9 Percent Fe	25	7.87	bcc
Molybdenum	99.9 Percent Mo	(a)	10.22	bcc
Titanium	Ti 5Al-2.5Sn	15	4.48	hcp

[a]Not measured.

TABLE 2. PHYSICAL PROPERTIES OF THE MINERAL OIL[a]

Density, kg/m^3	869
Kinematic viscosity at 20 °C, cS	110
Surface tension at 20 °C, dynes/cm	33.2
Bulk modulus, MPa	1.7×10^3
Flashpoint, °C	213
Pour point, °C	-9.4

[a]Drakeol 21 furnished by Penreco.

TABLE 3. - INCUBATION PERIODS, BEST FITTING EQUATIONS, AND STATISTICAL QUANTITIES

Material	Incubation period, t_0, min	Best fitting equation, $MDPN = AT^B$	Coefficient of determination, CD	Coefficient of correlation, CC	Standard error of estimate, SE
Al 6061-T6	1.3	$1.00\ T^{1.01}$	0.998	0.999	0.025
Cu (ETP)	.67	$1.00\ T^{1.14}$	.992	.996	.100
Brass	6.2	$1.00\ T^{1.52}$	.994	.997	.059
Phosphor bronze	16.5	$1.00\ T^{1.54}$	.993	.996	.077
Nickel	10.2	$1.00\ T^{1.73}$	.992	.996	.083
Iron	14	$1.00\ T^{1.76}$	.998	.999	.044
Molybdenum	270	$1.00\ T^{2.55}$	.994	.997	.068
Ti-5Al-2.5Sn	600	$1.00\ T^{1.03}$	.984	.992	.081

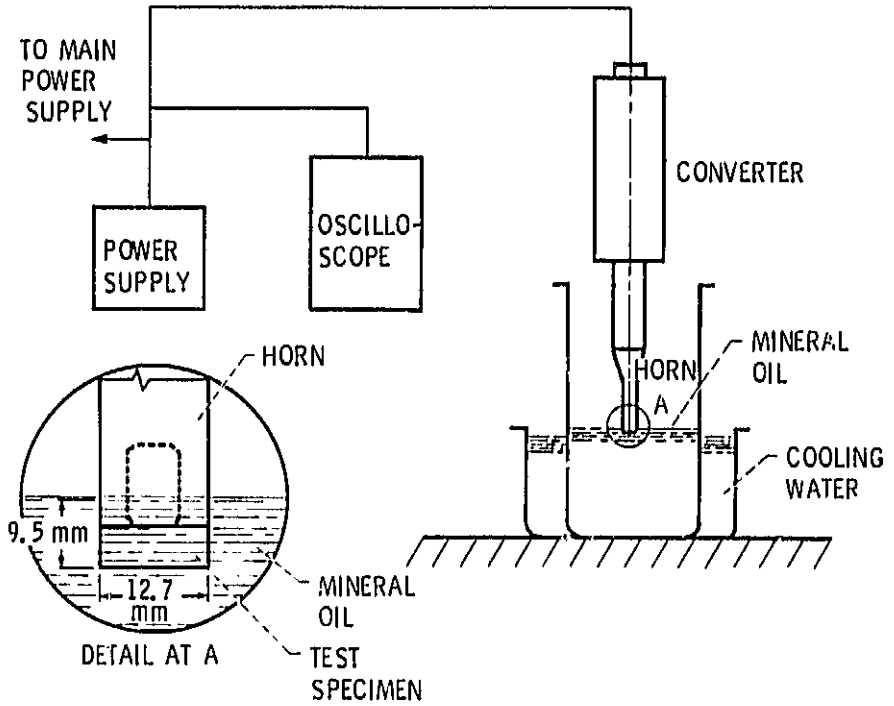

Figure 1. - Ultrasonic electrostrictive oscillator.

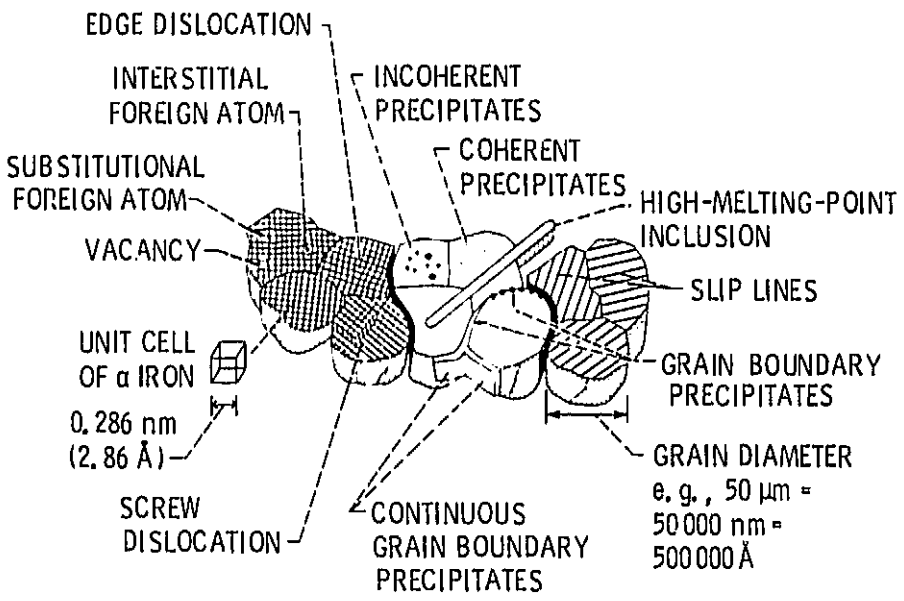

Figure 2. - Structure of a polycrystalline meta. . .d on example of iron. (From ref. 10.)

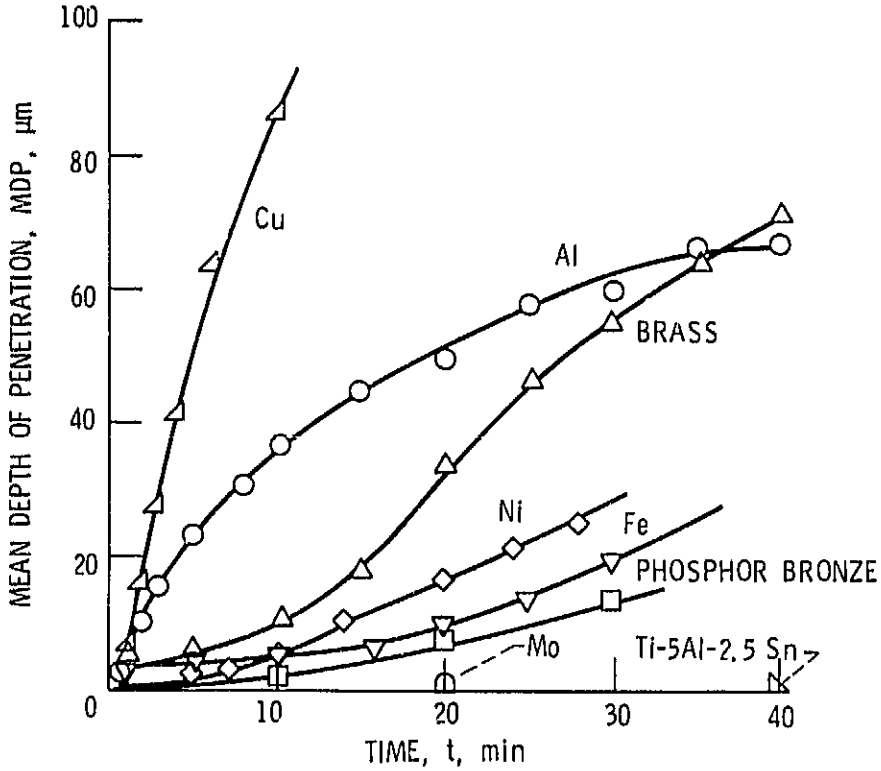

Figure 3. - Variation of mean depth of penetration with time - short test time.

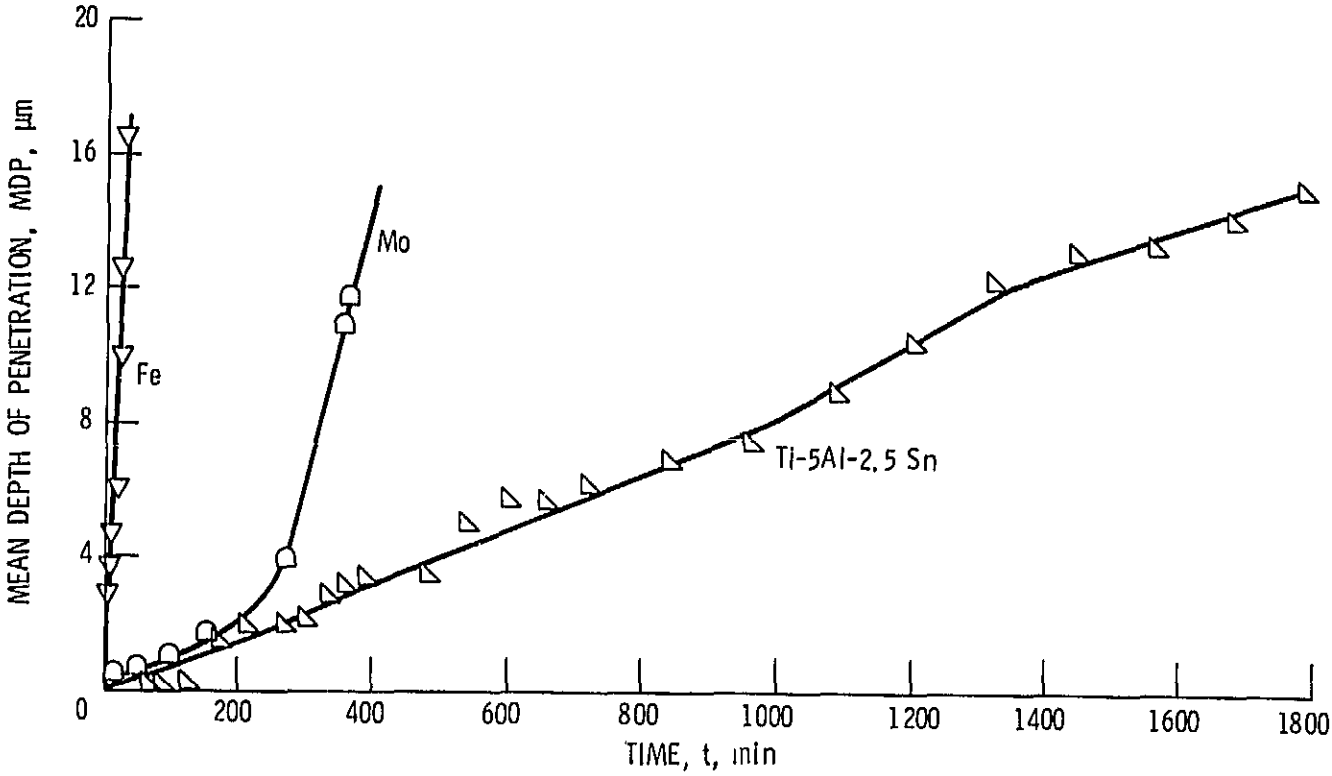

Figure 4. - Variation of mean depth of penetration with time - long test time.

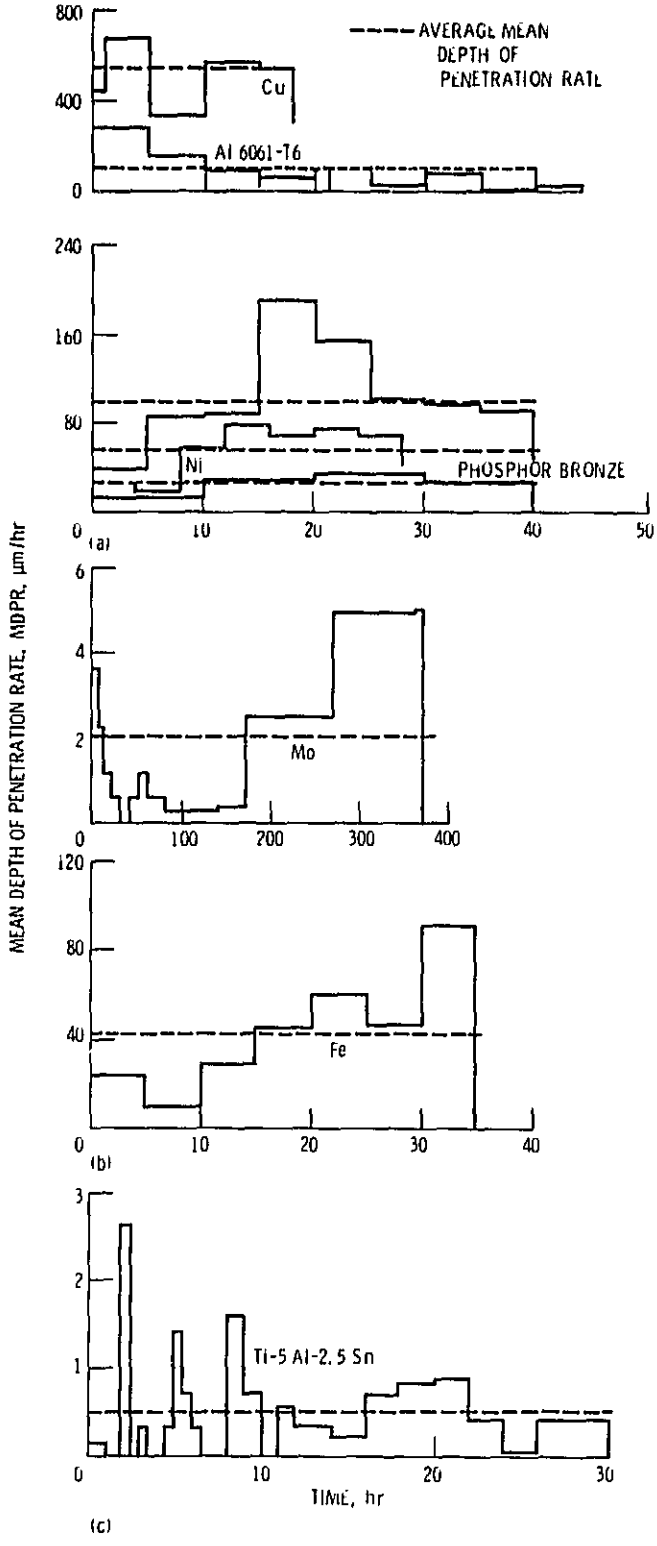

(a) fcc matrices.
(b) bcc matrices.
(c) hcp matrix.

Figure 5. - Variation of mean depth of penetration rate with time.

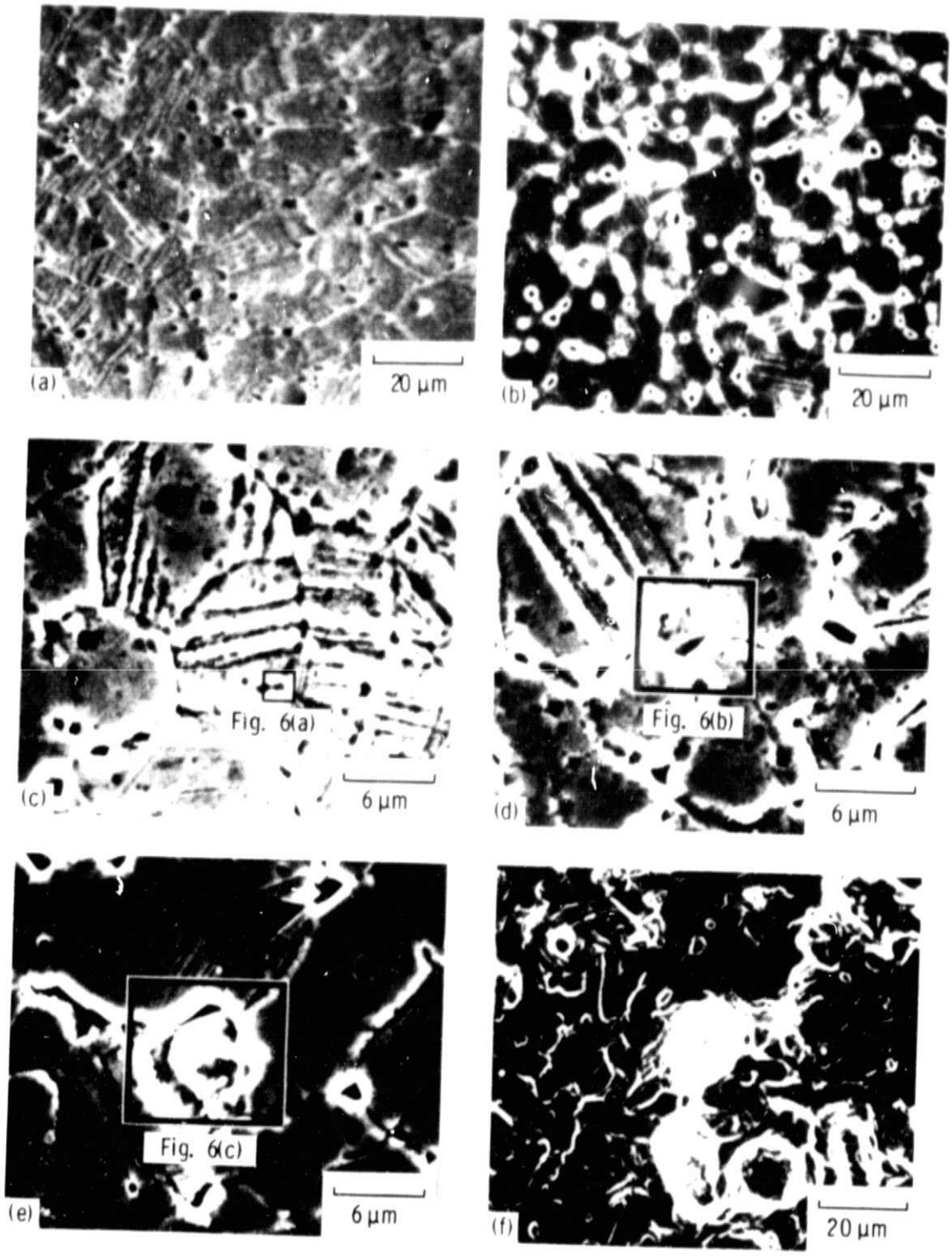

(a) Undamaged.
(b) t = 10 sec.
(c) t = 20 sec.
(d) t = 30 sec.
(e) t = 40 sec.
(f) t = 60 sec.

Figure 6. - SEM micrographs of brass surface.

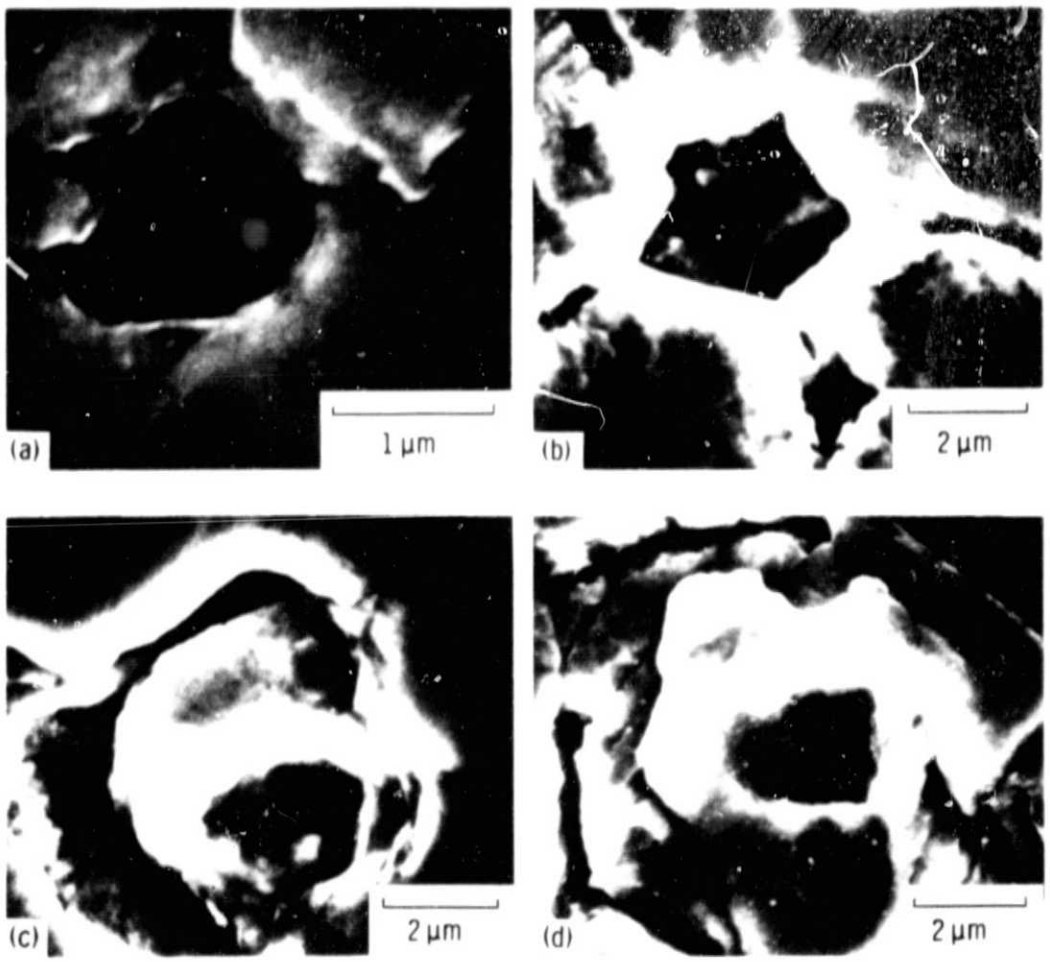

(a) t = 20 sec.
(b) t = 30 sec.
(c) t = 40 sec.
(d) t = 60 sec.

Figure 7. - Magnified views of cavitation attack on brass surface.

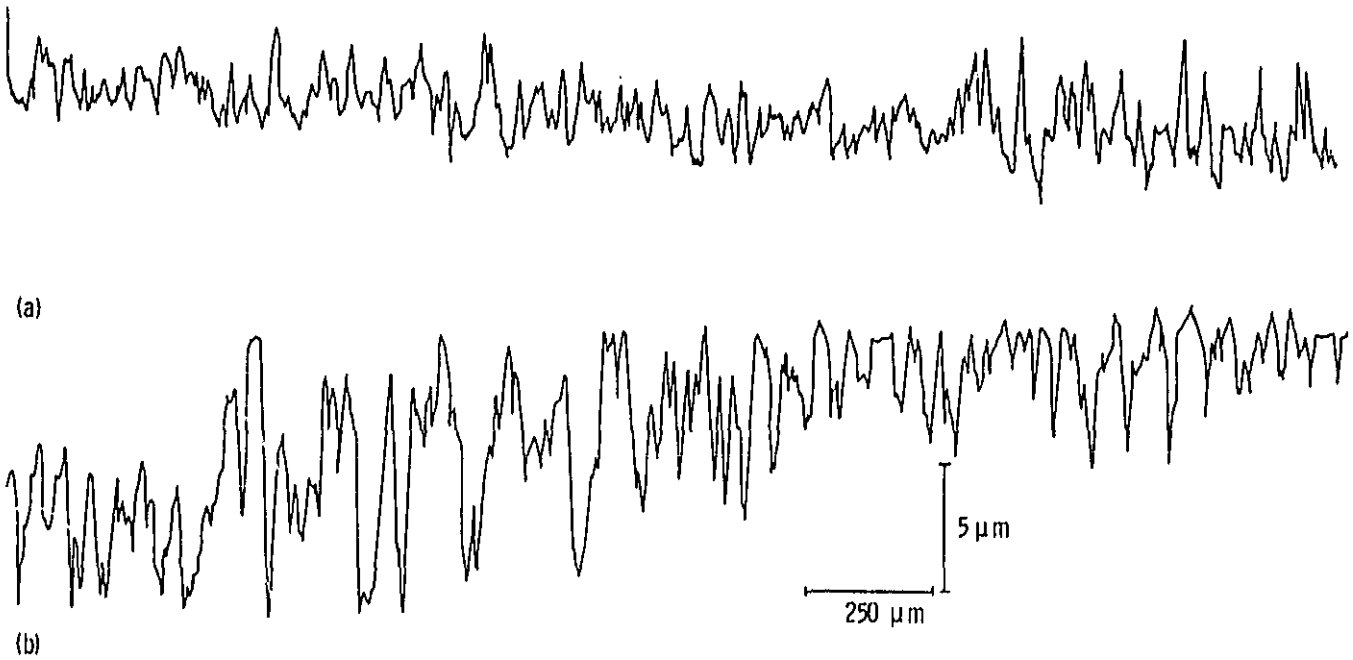

(a) t = 660 min. Maximum pit depth, h_{max}, ~6 μm.
(b) t = 1440 min. Maximum pit depth, h_{max}, ~9.5 μm.

Figure 8. - Surface profiles of Ti-5Al-2.5Sn specimen.

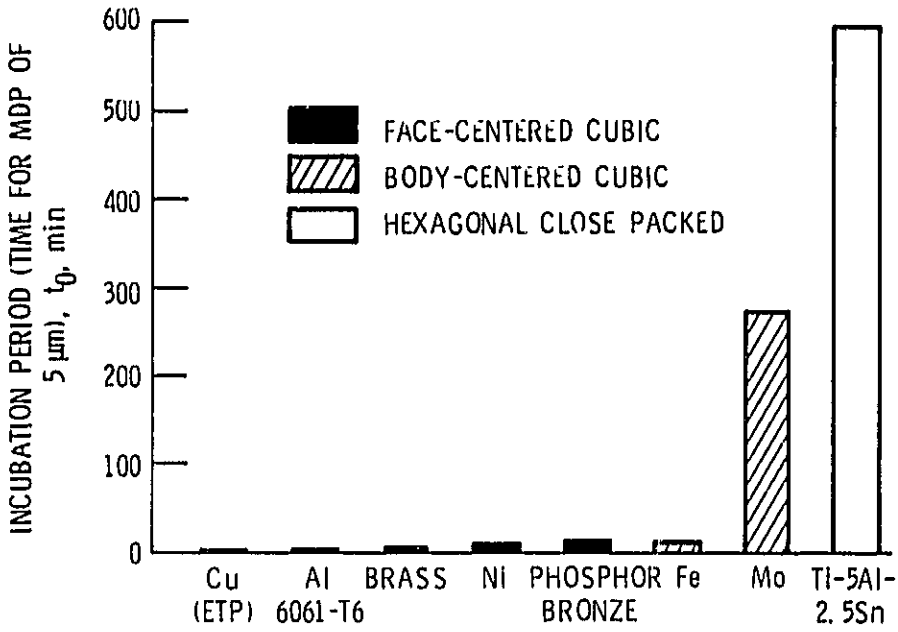

Figure 9. - Incubation periods of the metals studied.

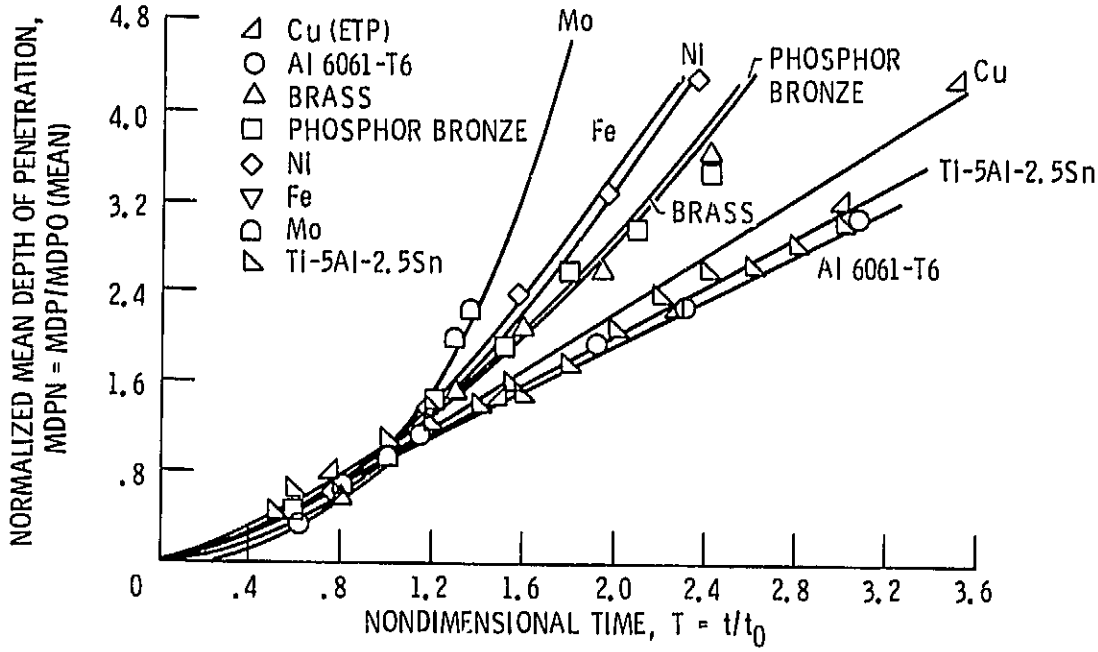

Figure 10. - Variation of nondimensional mean depth of penetration with nondimensional time.